Static Aeroelastic Characteristics of Circulation Control Wings

David J. Haas*
David Taylor Research Center, Bethesda, Maryland
and
Inderjit Chopra†
University of Maryland, College Park, Maryland

Circulation control airfoils can develop lift coefficients far in excess of conventional airfoils through the use of tangential blowing and thus have potential applications for V/STOL aircraft. The static aeroelastic effects of circulation control on swept wings are examined using two analytical models: a simple two-degree-of-freedom model with linearized aerodynamics and an elastic beam model coupled with nonlinear two-dimensional airfoil data. The static divergence instability and a circulation control reversal phenomenon are investigated through the use of lift and control effectiveness ratios. Effects of wing sweep angle, elastic axis location, blowing level, and spanwise blowing distribution are presented. Linear, nonlinear incompressible, and nonlinear compressible aerodynamic representations are compared. Significant differences were observed between the linear and nonlinear aerodynamic results. Tailoring of the spanwise blowing distribution is shown to be an effective means of improving undesirable aeroelastic characteristics. The results indicate that the aeroelastic behavior of circulation control wings can be quite different from that of conventional wings.

Nomenclature

$\mathcal{R}$ = wing aspect ratio, b/c
a = lift curve slope
b = wing span
CE = blowing control effectiveness
C_ℓ = section lift coefficient
C_L = wing lift coefficient
$C_{m_{1/2}}$ = section moment coefficient about midchord
C_{m_α} = $\partial C_{m_{1/2}}/\partial\alpha$
C_{m_μ} = $\partial C_{m_{1/2}}/\partial C_\mu$
C_μ = blowing momentum coefficient
ΔC_μ = increment in blowing momentum coefficient
C_{μ_0} = mean blowing momentum coefficient
c = chord
EI = bending stiffness
e = elastic axis offset in front of half-chord
GJ = torsional stiffness
K_β = bending spring constant
K_θ = torsion spring constant
LE = lift effectiveness
M = Mach number
q = free-stream dynamic pressure (at sea level)
S = wing area
V = free-stream velocity
Y = axis in spanwise direction
y_{cp} = spanwise location of wing center of pressure
α = total angle of incidence
α_0 = rigid angle of incidence
β = elastic bending rotation
ϵ = nondimensional offset of elastic axis from half-chord, positive forward
θ = elastic twist
Λ = wing sweep angle, positive aft
μ = lift augmentation ratio, $\partial C_\ell/\partial C_\mu$

Presented as Paper 87-0920-CP at the AIAA Dynamics Specialist Conference, Monterey, CA, April 9-10, 1987; received May 19, 1987; revision received June 7, 1988. This paper is declared a work of the U.S. Government and is not subject to copyright protection in the United States.

*Aerospace Engineer, Aviation Department. Member AIAA.
†Professor, Department of Aerospace Engineering. Associate Fellow AIAA.

Introduction

A TYPICAL circulation control (CC) airfoil is of quasi-elliptical shape with a sheet of air blown from a thin spanwise slot over a rounded trailing edge (Fig. 1). The jet of air remains attached over the curved trailing edge due to the Coanda effect and relocates the effective stagnation point toward the lower surface. Increasing the level of blowing changes the location of this stagnation point and thus can be used as a means to control the circulation of the airfoil. Performance of CC airfoils can be controlled by angle of attack as well as by jet momentum.

Lift augmentation through circulation control has been researched for many years at the David Taylor Research Center (DTRC).[1,2] The advantages of circulation control include the capabilities to attain high lift coefficients far in excess of conventional airfoils and to control lift independent of angle of attack. These unique performance characteristics make CC airfoils attractive for many V/STOL applications. For example, the Navy/Grumman A-6A flight demonstrator airplane and the Navy/Kaman XH2-CCR helicopter have both been flight tested with CC airfoils. In addition, stoppable rotors employing circulation control have been demonstrated successfully in wind-tunnel tests. The stoppable rotor concept embodies the cruise capability of a jet airplane (fixed-wing) and the hover capability of a helicopter (rotary-wing). These combined features are made possible through the application of CC technology. In this concept, the aircraft takes off and hovers like a helicopter and then, at a sufficient forward speed, the rotor is stopped to form a pair of forward- and aft-swept wings for flight as a fixed-wing aircraft. Circulation control is utilized to maintain vehicle control in all modes of flight: rotary wing, conversion, and fixed wing.

The potential of circulation control cannot be fully exploited on advanced aircraft configurations until its fundamental behavior, including aeroelastic interaction, is understood. Research has been quite limited in the important area of aeroelasticity for CC wings and blades. Chopra[3,4] has examined the dynamic stability of CC rotors in hover and forward flight, and Wilkerson[5] has studied wing divergence and CC reversal of unswept wings.

Considerable research is now being focused on the aeroelastic stability of forward-swept wings with conventional airfoils, including structural tailoring with composite materials.[6-9] Circulation control on forward- (and aft-) swept wings is of

interest particularly for stoppable rotor aircraft. In this paper the static aeroelastic characteristics of swept CC wings are examined. The wing is assumed to be an elastic beam undergoing bending and torsional deflections. Strip theory is used to obtain the aerodynamic forces, and the airfoil characteristics are expressed in terms of analytical expressions as well as two-dimensional data tables. Results are calculated for various parameters including wing sweep angle, elastic axis location, blowing level, and spanwise blowing distribution.

Circulation Control Aerodynamics

For a CC airfoil, the lift is a function of angle of attack as well as blowing level. Figure 2 shows the lift characteristics of a typical CC airfoil at low speeds. Unlike conventional airfoils, a CC airfoil can be assumed to consist of two aerodynamic centers – one due to angle of attack and the other due to blowing. The aerodynamic center due to angle-of-attack lift is located near the quarter-chord point (similar to a conventional airfoil), whereas the aerodynamic center due to jet momentum lift is located near the half-chord. For convenience, the aerodynamic moment coefficient for a CC airfoil is defined with respect to the half-chord position.

Note that as the blowing level on a CC airfoil is increased, the stall angle decreases. At maximum blowing levels a stall angle near or below zero deg angle of attack can occur. It is practical for CC airfoils to operate near the stall angle because stall occurs very gradually and a significant amount of lift can be attained even after the stall angle has been reached. Also, as shown in Fig. 2, lift coefficient varies with the blowing momentum coefficient, defined as

$$C_\mu = \dot{m}V_j/qc$$

where $\dot{m} = \rho A V_j$ is the mass flow of air through the slot, V_j the jet velocity, and q the dynamic pressure normal to the wing leading edge. Blowing momentum coefficient C_μ is essentially determined by the duct pressure P_d (controlled by the pilot) and the slot height-to-chord ratio h/c (an airfoil design parameter). Since the dynamic pressure q appears in the denominator, large values of the blowing coefficient can generally be attained only at low speeds. The variation of available C_μ vs Mach number is shown in Fig. 3 for a typical compressor capable of producing a pressure ratio of 2.1. Due to the rapid decrease in available C_μ at higher speeds, circulation control functions as a high-lift augmentation system only in the low-speed range (takeoff and landing). At the high-speed flight condition, blowing would be used primarily for vehicle control. In all of the results presented, it is assumed that the vehicle control system regulates the duct pressure such that C_μ remains constant with forward speed. Because of the high-speed limitations on available C_μ, relatively low values of blowing are used in the examples.

A two-dimensional airfoil data base from wind-tunnel model tests exists at DTRC for CC airfoils of various combinations of thickness-to-chord ratio, camber, slot height, slot location, and trailing-edge profile (Coanda surface). Section properties in tabular form are available over a wide range of α and C_μ at subsonic to transonic speeds. For the present study, the airfoil characteristics from these data tables are used to calculate aerodynamic forces on the wing.

Analytical Model

Simple two-degree-of-freedom (DOF) models have long been useful as learning tools and as a first analytical approach in the study of aeroelastic phenomenon. Even recently, two-DOF models have provided insight into the understanding of transonic aeroelastic stability and the use of stiffness cross-coupling with composite materials to alleviate flutter and static divergence.[8] Wilkerson[5] used an even simpler single-DOF torsion model to study divergence and CC reversal on unswept CC wings.

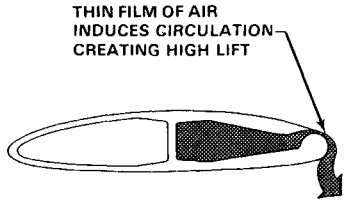

Fig. 1 Typical circulation control airfoil.

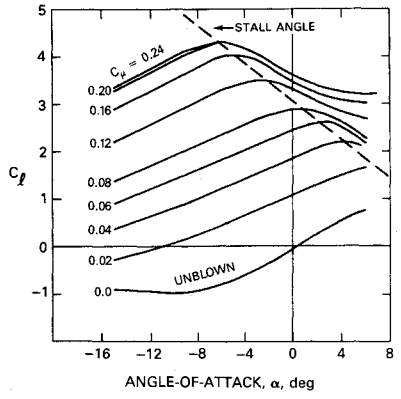

Fig. 2 Lift characteristics of a typical circulation control airfoil.

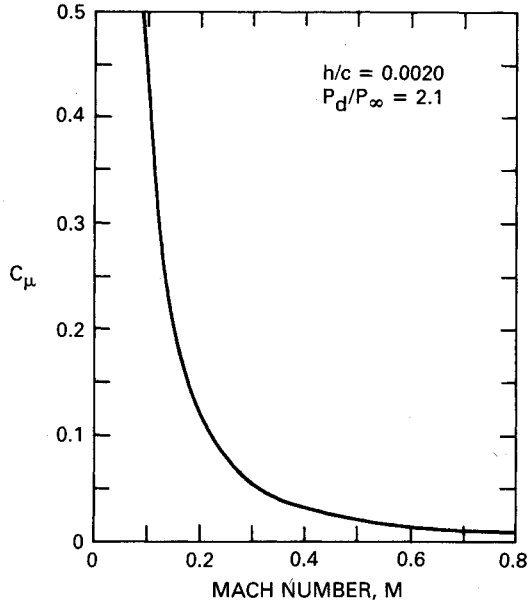

Fig. 3 Available blowing momentum coefficient.

In this study, two analytical models are used to examine the aeroelastic behavior of a CC wing. The first is a two-DOF model (similar to the one in Ref. 8) with linearized aerodynamics. The second is an elastic beam model coupled with nonlinear airfoil data (see Fig. 4).

Two-DOF Model

In the two-DOF model (Fig. 4a), the wing is assumed to be rigid and supported at the root by two springs with stiffnesses K_β and K_θ which allow bending rotation β and torsional rotation θ, respectively. The sweep angle Λ of the wing is taken positive aft.

Strip theory is used to obtain the aerodynamic forces and the airfoil characteristics are represented by linear expressions as

$$C_\ell = C_{\ell_0} + a\alpha + \mu C_\mu \tag{1a}$$

$$C_{m_{1/2}} = C_{m_0} + C_{m_\alpha}\alpha + C_{m_\mu}C_\mu \tag{1b}$$

These coefficients are obtained from a curve fit to the experimental data. The lift augmentation ratio μ is defined as the change in lift coefficient due to a given change in blowing momentum coefficient. In this model, the angle of attack α is the same for all spanwise stations and depends on the elastic rotations β and θ as

$$\alpha = \alpha_0 + \theta - \beta \tan\Lambda \tag{2}$$

where α_0 is the rigid angle of attack. The bending and torsion moment equilibrium equations for the wing are

$$\left(\begin{bmatrix} K_\beta & 0 \\ 0 & K_\theta \end{bmatrix} - \begin{bmatrix} K_a \end{bmatrix}\right)\begin{Bmatrix} \beta \\ \theta \end{Bmatrix} = \begin{Bmatrix} M_\beta \\ M_\theta \end{Bmatrix}_{\text{rigid}} \tag{3}$$

where components of the aerodynamic stiffness matrix K_a are defined as

$$K_{a_{11}} = -\bar{q}ay_{cp}\tan\Lambda$$

$$K_{a_{12}} = \bar{q}ay_{cp}$$

$$K_{a_{21}} = \bar{q}ac\,(\epsilon - C_{m_\alpha}/a)\tan\Lambda$$

$$K_{a_{22}} = -\bar{q}ac\,(\epsilon - C_{m_\alpha}/a)$$

$$\bar{q} = qS\cos^2\Lambda$$

y_{cp} = spanwise center of pressure location

Here, positive ϵ is the nondimensional elastic axis offset in front of the half-chord point ($\epsilon = e/c$). The wing aerodynamic moments due to α_0 are

$$M_{\beta_{\text{rigid}}} = \bar{q}y_{cp}\,(C_{\ell_0} + \mu C_\mu + a\alpha_0)$$

$$M_{\theta_{\text{rigid}}} = \bar{q}c\,(C_{m_0} + C_{m_\mu}C_\mu + C_{m_\alpha}\alpha_0) - \bar{q}c\epsilon\,(C_{\ell_0} + \mu C_\mu + a\alpha_0)$$

For a prescribed q, Eq. (3) can be solved for elastic rotations β and θ.

Lift effectiveness and control effectiveness are useful ratios that characterize the static aeroelastic response of an elastic wing. Lift effectiveness (LE) is defined as the lift of an elastic wing divided by the lift of an equivalent rigid wing. For the two-DOF model with linear aerodynamic representation, this effectiveness ratio can be expressed in a simple form. Using Eqs. (1) and (2),

$$\text{LE} = 1 + \frac{a(\theta - \beta\tan\Lambda)}{(C_{\ell_0} + a\alpha_0 + \mu C_\mu)} \tag{4}$$

For an unswept wing ($\Lambda = 0$), torsion deformation is decoupled from bending, and divergence occurs when elastic twist θ approaches infinity. For a forward swept wing ($\Lambda < 0$), divergence occurs when bending deformation β approaches infinity. This can happen even when the wing is infinitely stiff in torsion. In all cases, lift effectiveness will approach infinity at the static divergence condition.

The control effectiveness (CE) for a CC wing is defined as the change in lift due to a given change in blowing momentum coefficient for an elastic wing divided by the corresponding quantity of an equivalent rigid wing, as

$$\text{CE} = \frac{[C_L(\alpha, C_{\mu_0} + \Delta C_\mu) - C_L(\alpha, C_{\mu_0})]_{\text{elastic}}}{[C_L(\alpha, C_{\mu_0} + \Delta C_\mu) - C_L(\alpha, C_{\mu_0})]_{\text{rigid}}} \tag{5}$$

where C_{μ_0} is the mean blowing momentum coefficient and ΔC_μ is the increase in the blowing level. For the linear case, this can be expressed in simple form by taking derivatives with respect to C_μ of the numerator and denominator in Eq. (4), as

$$\text{CE} = 1 + \frac{a}{\mu}\left(\frac{\partial\theta}{\partial C\mu} - \frac{\partial\beta}{\partial C_\mu}\tan\Lambda\right) \tag{6}$$

The partial derivatives of θ and β with respect to C_μ in Eq. (6) are evaluated by solving Eq. (3) for θ and β and differentiating the resulting equations. Circulation control reversal is defined as the condition where CE goes to zero. At speeds beyond this point, an increase in blowing level would result in a decrease in total wing lift.

Elastic Beam Model

The wing is assumed to be an elastic beam clamped at the root undergoing elastic twist and bending deflections (Fig. 4b). This idealization is a good representation for large-aspect ratio-wings. A lumped parameter formulation is adopted to study the interaction of elastic and aerodynamic forces. The wing is divided into a number of spanwise strips and the flexibility influence coefficients at various points are calculated analytically. The elastic axis is assumed to be a straight line and normal to the effective root. Aerodynamic forces are obtained using a strip theory approach with two-dimensional experimental airfoil properties (tabular data). Finite span effects are neglected.

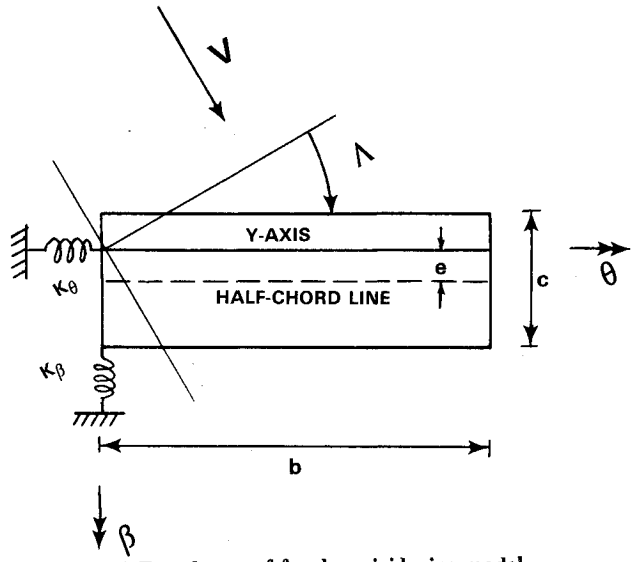

a) Two-degree-of-freedom rigid wing model

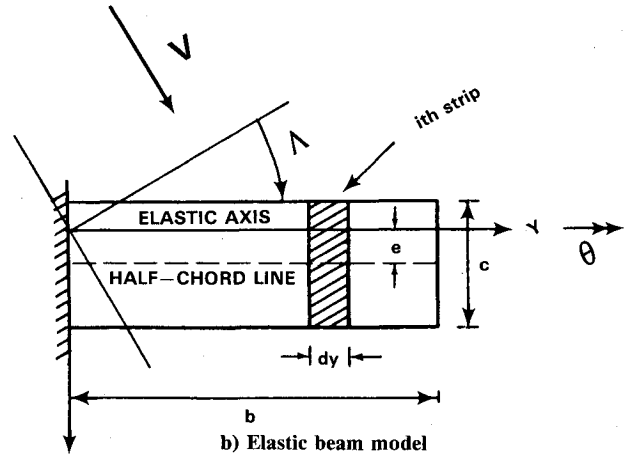

b) Elastic beam model

Fig. 4 Analytical models.

The vertical displacement vector w and the elastic twist vector θ can be expressed in matrix form as

$$\begin{Bmatrix} w \\ \theta \end{Bmatrix} = \begin{bmatrix} C \end{bmatrix} \begin{Bmatrix} L \\ M \end{Bmatrix} \tag{7}$$

where C is the matrix of structural influence coefficients derived from linear beam theory. The vectors L and M represent aerodynamic lift and torsional moment about the elastic axis acting at various strips. For an ith strip,

$$L_i = q \cos^2\Lambda \, (C_\ell c\,dy)_i \tag{8}$$

$$M_i = q \cos^2\Lambda \, (C_{m_{1/2}} c\,dy - \epsilon C_\ell c\,dy)_i \tag{9}$$

The aerodynamic coefficients C_ℓ and $C_{m_{1/2}}$ are taken from data tables and are nonlinear functions of angle of attack α, blowing momentum coefficient C_μ, and Mach number M. The Mach number is determined from the component of velocity normal to the wing. The angle of attack of the ith strip can be expressed using classical sweep theory as

$$\alpha = \alpha_0 + \theta_i - (dw/dy)_i \tan\Lambda \tag{10}$$

The vector of local bending slopes is evaluated in terms of the vertical displacement vector w using a numerical weighting matrix. Equation (7) is a set of nonlinear equations that must be solved iteratively for w and θ. With elastic deformation known, total lift and moment can be determined by substitution into Eqs. (8–10). Elastic displacements are set equal to zero to determine rigid wing lift and effectiveness ratios and then evaluated directly from their definitions.

Results and Discussion

Numerical results are calculated for a CC wing with trailing-edge blowing (single slot). The wing is assumed to be uniform along the span. Structural and aerodynamic properties are given in Tables 1 and 2. A 15% quasi-elliptic airfoil is chosen because it is representative of an outboard section on a stoppable rotor aircraft. For the baseline configuration, the elastic axis is assumed to be at the half-chord position and the rigid angle of incidence is 2 deg. Results are presented for the simple two-DOF wing using a linear aerodynamic model and for the elastic beam model using nonlinear aerodynamic characteristics.

Two-DOF Model (Linear)

The linear model is used to qualitatively show the effect of wing sweep and blowing level on LE and CE. Results are calculated for three wing sweep angles: 0 deg (unswept), −45 deg (swept forward), and 45 deg (swept aft). Compressibility effects are neglected for the two-DOF model results and the aerodynamic coefficients C_{ℓ_0}, C_{m_0}, and C_{m_μ} are assumed to be zero. This assumption represents an idealization that the only effect of blowing is to produce lift exactly at the half-chord point.

Table 1 Properties of baseline wing

AR	10	K_β/K_θ	6.2
S	90 ft	EI	30.0×10^6 lb-ft^2
b	30 ft	EI/GJ	4.0
e	0.0 ft	α_0	2 deg

Table 2 Aerodynamic characteristics used with two-DOF model

15% Quasi-elliptic airfoil			
Slot location	0.97c	C_{m_α}	1.25
h/c	0.0015	C_{ℓ_0}, C_{m_0}, C_{m_μ}	0.0
a	5.0	y_{cp}	15.0 ft
μ	55.0		

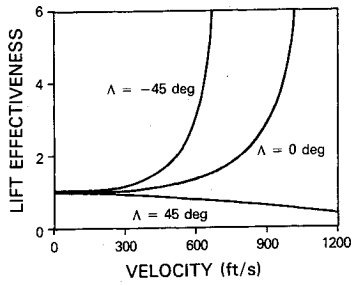

Fig. 5 Lift effectiveness with no blowing using two-DOF linear model.

Figure 5 shows lift effectiveness for the wing with a zero blowing condition and an angle of incidence α_0 equal to 2 deg. Lift effectiveness defines the ratio of elastic wing lift to rigid wing lift for a set angle of incidence. A value greater than one shows that an additional positive lift is being produced by wing deflections. At the critical divergence instability, LE will approach infinity. As expected, forward sweep reduces the speed at which LE approaches infinity (i.e., reduces static divergence speed) because the wing bending introduces additional elastic lift. The opposite effect occurs with aft sweep, where the wing becomes free from divergence instability since the LE is less than unity for all speeds.

The elastic axis location was also varied for each of these cases, but had a pronounced effect only on the unswept wing. This is because the elastic lift for an unswept wing is due only to elastic twist; wing bending plays no role. For a nonblowing condition, lift acts at the quarter-chord; hence, bringing the elastic axis closer to this position on the unswept wing reduces elastic lift and, therefore, increases the divergence speed (see Ref. 10 for additional results).

When blowing is added, the resultant aerodynamic center moves aft of the quarter-chord position, which changes the LE curve (Fig. 6). However, divergence speed does not change with blowing; instead, blowing affects the growth rate of elastic lift before divergence occurs. For example, in Fig. 6, with the elastic axis at the midchord position, increasing the level of blowing reduces LE, but causes a sharper penetration into the divergence condition. Similar behavior is observed on the LE of swept wings due to blowing.

Figure 7 presents the effect of wing sweep on blowing control effectiveness. This ratio shows the effectiveness of blowing to increase lift. A value of CE less than one indicates that the lift change due to blowing has been reduced due to elastic deflections caused by the blowing. Zero CE represents the critical condition where blowing has no control on lift. A negative value would result in control reversal; i.e., increasing the blowing level would reduce total lift. For the swept-forward wing, the bending deflections do not let control effectiveness fall below one, thus removing the possibility of control reversal. This phenomenon works somewhat contrary to wing divergence, which worsens on swept forward wings. However, for the aft-swept wing CE decreases rapidly with forward speed.

As with LE, the elastic axis location has little effect when the wing is swept forward or aft by 45 deg because wing bending behavior is dominant. However, for the unswept wing, the elastic axis position plays an important role. When the elastic axis is located behind the half-chord, the wing will not experience control reversal. If the elastic axis is located in front of the half-chord, control reversal will occur. This is because the aerodynamic center due to blowing lift is located at the half-chord. In addition, for the unswept wing, the exact position of the elastic axis ahead of the half-chord does not change the actual reversal speed, but instead only the penetration rate into the reversal condition. A quick penetration would give no warning to the pilot and can be dangerous. Note from Eq. (6) that CE does not depend on the mean blowing level with the linear model.

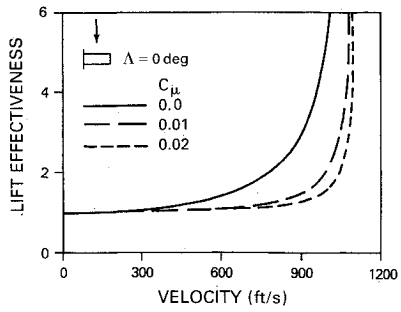

Fig. 6 Effect of blowing level on lift effectiveness for unswept wing using two-DOF linear model.

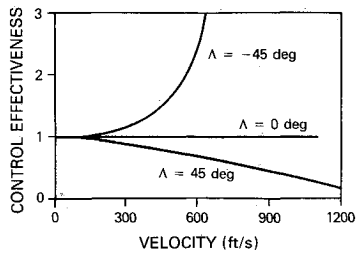

Fig. 7 Control effectiveness using two-DOF linear model ($C_{\mu_0} = 0$, $\Delta C_\mu = 0.005$).

Elastic Beam Model (Nonlinear)

The nonlinear model is used to investigate the influence of aerodynamic modeling. The effects of nonlinear aerodynamics and compressibility are determined by using data tables for the airfoil characteristics. For comparison, a linear aerodynamic representation is also used with the elastic beam model. However, for this case, all of the coefficients in Eqs. (l) are linearized directly from the data table. In addition, several parameters that influence LE and CE are examined, including the spanwise blowing distribution.

Figure 8 shows the effect of aerodynamic modeling on the LE of an unswept wing with the blowing level set to zero and an elastic axis located at the half-chord. The wing incidence is initially set at 2 deg. For the linear model (stall neglected), it is easy to define the divergence stability boundary because LE approaches infinity. However, the LE does not diverge to infinity with nonlinear airfoil characteristics, but reaches some maximum value, levels off, and then begins to decrease. The reason for this behavior is that, as the wing twists with increasing forward speed, the stall angle of attack is reached. At that point, the lift curve slope becomes negative, resulting in a decrease in elastic lift. For a nonlinear model, a large value of LE represents an uncontrollable condition and thus must be avoided. There is an appreciable influence of compressibility on LE for high-subsonic speeds ($M > 0.6$), perhaps because of an increased lift curve slope (Prandtl-Glauert correction). The maximum value of LE is about 3.6 for compressible flow and about 2.9 for incompressible flow.

Figure 9 shows the effect of aerodynamic modeling on the blowing control effectiveness for the same wing. Again, the influence of compressibility is quite significant. In fact, with compressibility included there is a more rapid decrease of CE with speed. Furthermore, the linear theory predicts a much smaller change in CE from a value of one for this configuration, whereas the nonlinear theory shows a significant reduction in blowing CE at higher speeds ($V > 700$ ft/s). Therefore, linear theory overpredicts LE and underpredicts the decrease in CE with speed for this configuration, as shown in Figs. 8 and 9. On the forward- and aft-swept wings, compressibility effects are less pronounced because the normal Mach number is much lower. Subsequent results are calculated using the nonlinear compressible airfoil data.

The effect of elastic axis location on LE for an unswept wing with no blowing is shown in Fig. l0a. These results are similar to linear results in that the critical speed, where LE changes abruptly, increases as the elastic axis is brought closer to the quarter-chord position. The effect of blowing on LE is illustrated in Fig. l0b for the unswept wing with an elastic axis located at the half-chord. The LE is calculated for three values of blowing momentum. With blowing, the LE ratio is significantly reduced because the lift due to elastic twist is

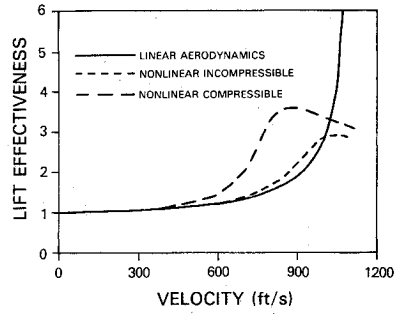

Fig. 8 Influence of aerodynamic modeling on lift effectiveness for unswept wing with no blowing.

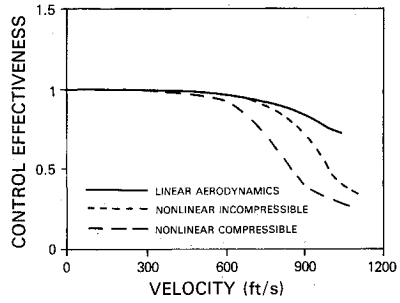

Fig. 9 Influence of aerodynamic modeling on control effectiveness for unswept wing ($C_{\mu_0} = 0$, $\Delta C_\mu = 0.005$).

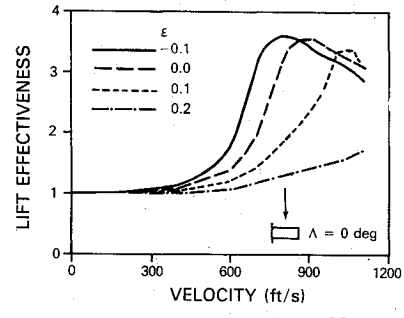

a) Effect of elastic axis location for unblown case

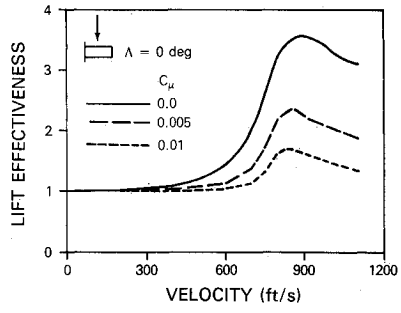

b) Effect of blowing with half-chord elastic axis location

Fig. 10 Lift effectiveness for unswept wing.

proportionally much less than for the unblown wing. A somewhat similar observation was made with the linear two-DOF model (Fig. 6). Furthermore, once the wing begins to stall, lift due to elastic deformation no longer increases as rapidly, which results in a "leveling off" and then a decrease in LE. To further illustrate this phenomenon, the wing is swept forward 45 deg (where divergence instability is most critical). Figure 11 shows the LE for various amounts of blowing. At the highest blowing level, LE is nearly constant with forward speed. For all values of blowing, elastic deformations remain within the range of linear beam theory and thus do not indicate structural failure of the wing. However, the unblown case may represent an uncontrollable condition because a rapid amplification of LE takes place.

Control effectiveness defines the response of an elastic wing to an increase in blowing above some mean value. For the subsequent examples, CE is calculated by increasing the mean blowing coefficient C_{μ_0} by the amount ΔC_μ, which equals 0.005.

The CE for a 45 deg aft-swept wing with a half-chord elastic axis location is shown in Fig. 12. A rapid decrease in CE is indicated, which worsens as C_{μ_0} is increased. For this elastic axis location, reversal does not occur; instead CE drops quickly to about 0.4 and then reduces more slowly thereafter. For the 45 deg forward-swept wing (Fig. 13) with C_{μ_0} equal to zero, the CE initially increases with speed and then rapidly decreases. This rapid decrease in CE is caused by stall conditions resulting from the elastic deformations induced by ΔC_μ. When a larger value of C_{μ_0} is used, this phenomenon disappears because LE is much less at this condition. Thus, the CE on a forward-swept wing calculated from the nonlinear model is quite different from that obtained using the linear model (Fig. 7). The unswept wing behaves quite similarly to the 45 deg aft-swept wing.

Finally, tailoring of the spanwise blowing distribution to minimize undesirable aeroelastic effects is investigated. Three different types of distributions are used: uniform ($C_\mu = 0$ .005), linearly increasing C_μ from zero at the root to 0.01 at the tip, and linearly decreasing C_μ from 0.01 at the root to zero at the tip. The half-chord point is chosen for the elastic axis location in the following examples. Amplification of LE ratio is the primary concern for wings with large forward sweep angles. Figure 14 illustrates the effect of spanwise blowing distribution on a 45 deg swept-forward wing. A slight decrease in maximum LE is attained with the linearly increasing C_μ distribution because the additional blowing at the wing tip creates greater wing bending. This, in turn, increases the effective angle of attack, causing the wing to stall earlier and thus lowering the LE.

In contrast to forward-swept wings, loss of CE is the critical condition on aft-swept wings. In Fig. 15, CE is shown for a 45 deg aft-swept wing with three different blowing distributions. For this example, CE is based on a C_{μ_0} equal to zero and the following prescribed spanwise distributions of ΔC_μ: uniform ($\Delta C_\mu = 0.005$), linearly increasing ΔC_μ from zero at the root to 0.01 at the tip, and linearly decreasing ΔC_μ from 0.01 at the root to zero at the tip. From the results, it is evident that a linearly decreasing ΔC_μ distribution can significantly improve CE. Conversely, a linearly increasing ΔC_μ distribution can substantially decrease CE and even cause a reversal condition at high speeds. On the aft-swept wing, an outboard load causes larger bending deflection, which decreases the angle of attack and in turn negates some of the effect of blowing. An inboard blowing distribution on an aft-swept wing is therefore desirable from a CE standpoint.

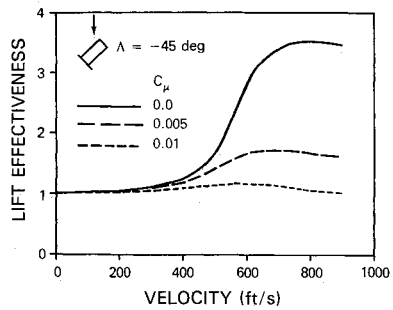

Fig. 11 Lift effectiveness for forward-swept wing.

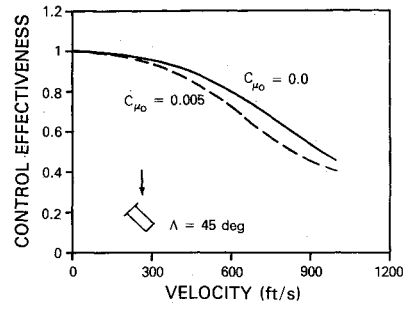

Fig. 12 Effect of mean blowing level on control effectiveness for aft-swept wing.

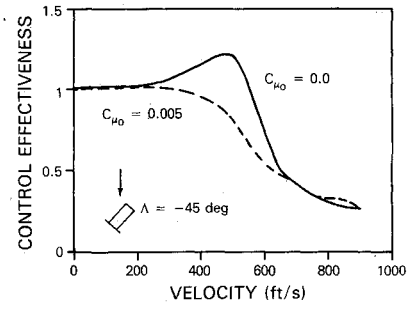

Fig. 13 Effect of mean blowing level on control effectiveness for forward-swept wing.

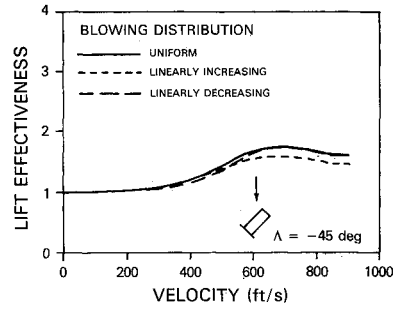

Fig. 14 Effect of spanwise blowing distribution on lift effectiveness for forward-swept wing.

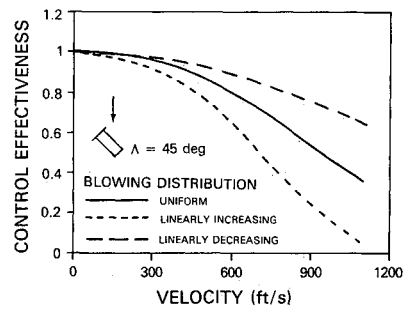

Fig. 15 Effect of spanwise blowing distribution on control effectiveness for aft-swept wing ($C_{\mu_0} = 0$).

Summary and Conclusions

For swept-forward wings with conventional airfoils, large values of lift effectiveness can occur at high speed, which may result in catastrophic deformations (wing divergence). Thus, a conservative approach must be used to design the divergence speed well outside the flight envelope. The nonlinear results of the swept-forward circulation control wing in this study show that values of lift effectiveness large enough to cause structural failure did not occur. Instead, stall conditions occurred at low angle of attack, thus preventing a catastrophic buildup in lift effectiveness. However, on the unblown CC wing a significant amplification in lift effectiveness did occur. Therefore, divergence on a CC wing may be characterized by an uncontrollable condition where vehicle trim is difficult to maintain due to rapid changes in total lift.

For a stoppable rotor configuration, 45 deg swept-forward and 45 deg swept-aft CC wings are joined at the root. Applying the results of this investigation (ignoring any wing interaction effects) to this configuration indicates that an aeroelastic pitch-up moment will develop with increasing forward speed. This moment arises due to the increasing lift effectiveness on the forward-swept wing and the decreasing lift effectiveness on the aft-swept wing. Because structural symmetry must be maintained, aeroelastic tailoring with composites cannot be used to alleviate this effect. Also, this moment may be difficult to react at high speeds using differential wing blowing due to the loss in control effectiveness on the aft-swept wing. The designer should be aware of this when sizing the horizontal tail on a stoppable rotor aircraft.

The aerodynamic and structural interactions for circulation control wings were investigated. Static divergence was studied through the use of a lift effectiveness ratio. Alternately, a blowing control effectiveness ratio was defined to assess the response of an elastic wing to a control input of increased blowing. The effects of nonlinear aerodynamics and compressibility were significant and should be included for static aeroelastic analysis of CC wings.

The following are conclusions concerning lift effectiveness and static divergence for the numerical examples presented in this study:

1) A simple two-degree-of-freedom model provides an approximate qualitative picture of lift effectiveness.

2) With the nonlinear aerodynamic model, divergence (i.e., lift effectiveness approaching infinity) does not occur; however, an amplification of lift effectiveness takes place that is limited due to airfoil stall.

3) Increasing the blowing level reduces lift effectiveness.

4) Forward sweep increases lift effectiveness, thus lowering divergence speed.

5) The elastic axis location has a significant influence for unswept wings, but only a comparatively small effect for swept wings.

6) A linearly increasing distribution of spanwise blowing can reduce lift effectiveness (as compared to the uniform blowing distribution) on forward-swept wings at the expense of larger tip deflections.

Conclusions concerning control effectiveness are:

7) Aft sweep reduces control effectiveness.

8) Elastic axis location has only a slight influence for aft-swept wings.

9) Increased mean blowing level can reduce control effectiveness.

10) A linearly decreasing distribution of spanwise blowing can significantly improve control effectiveness on an aft-swept wing.

None of the results presented preclude the use of circulation control on swept wings for static aeroelastic reasons. To the contrary, circulation control wings may be more desirable than conventional wings from a divergence standpoint. However, in order to gain maximum benefit from circulation control, the designer must be aware of its impact on aeroelastic behavior.

References

[1]Englar, R. J. and Applegate, C. A., "Circulation Control – A Bibliography of DTNSRDC Research and Selected Outside References," DTNSRDC Rept. 84-052 (AD A146-966), Sept. 1984.

[2]Rogers, E. O., Schwartz, A. W., and Abramson, J. S., "Applied Aerodynamics of Circulation Control Airfoils and Rotors," Paper Presented at 11th European Rotorcraft Forum, London, Sept. 1985.

[3]Chopra, I., "Dynamic Stability of a Bearingless Circulation Control Rotor Blade in Hover," *Journal of the American Helicopter Society*, Vol. 30, Oct. 1985, pp. 40–47.

[4]Chopra, I., "Aeroelastic Stability of a Bearingless Circulation Control Rotor in Forward Flight," *Journal of the American Helicopter Society*, Vol. 33, July 1988, pp. 60–67.

[5]Wilkerson, J. B., "Aeroelastic Characteristics of a Circulation Control Wing," DTNSRDC Rept. 76-0115 (AD A033-328), Sept. 1976.

[6]Shirk, M. H., Hertz, T. J., and Weisshaar, T. A., "Aeroelastic Tailoring – Theory, Practice, and Promise," *Journal of Aircraft*, Vol. 23, Jan. 1986, pp. 6–18.

[7]Lottati, I., "Flutter and Divergence Aeroelastic Characteristics for Composite Forward Swept Cantilevered Wing," *Journal of Aircraft*, Vol. 22, Nov. 1985, pp. 1001–1007.

[8]Weisshaar, T. A. and Ryan, R. J., "Control of Aeroelastic Instabilities through Stiffness Cross-Coupling," *Journal of Aircraft*, Vol. 23, Feb. 1986, pp. 148–155.

[9]Landsberger, B. J. and Dugundji, J., "Experimental Aeroelastic Behavior of Unswept and Forward-Swept Cantilever Graphite/Epoxy Wings," *Journal of Aircraft*, Vol. 22, Aug. 1985, pp. 679–682.

[10]Haas, D. J. and Chopra, I., "Aeroelastic Characteristics of Swept Circulation Control Wings," AIAA Paper 87-0920, April 1987.